VGOS Technology R&D Sessions

B. Petrachenko[1], M. Schartner[2], M. Xu[3,4]

Abstract A series of VGOS technology R&D sessions has been undertaken. In total, seven 24-hour sessions were scheduled along with associated 1-hour tests. The primary goal is to significantly increase the number of observations per session at each station. In the VGOS R&D series so far, the number of observations per session has more than doubled when compared to current operational VGOS sessions. Other related priorities include: 1) to optimize high rate schedules both for geodesy and for imaging; 2) to develop and test processes to determine and apply source structure corrections; and 3) to evaluate and test improved frequency sequences. Sources were analyzed to produce closure images, maps, models, and preliminary corrections.

Keywords VGOS, Technology, VTC, R&D

1 Introduction

In early 2021 the IVS Observing Program Committee (OPC) informed the VGOS Technical Committee (VTC) that resources had been allocated for a series of VGOS technology R&D sessions. Within this mandate, a series of seven 24-hour VGOS R&D sessions were undertaken along with associated 1-hour tests. The main purpose of the sessions is to demonstrate operational readiness for "high rate observing," in other words, to move towards the VLBI2010 target [2] of, on average, one scan every 30 seconds at each station. Other related priorities include: 1) to optimize high rate schedules both for geodesy and for imaging; 2) to develop and test processes to determine and apply source structure corrections; and 3) to evaluate and test improved frequency sequences.

1. Natural Resources Canada (retired), Canada
2. Institute of Geodesy and Photogrammetry, ETH Zürich, Robert-Gnehm-Weg 15, CH-8093 Zurich, Switzerland
3. Aalto University Metsähovi Radio Observatory, Metsähovintie 114, FI-02540 Kylmälä, Finland
4. Aalto University Department of Electronics and Nanoengineering, PL15500, FI-00076 Aalto, Finland

2 The Sessions

A total of seven 24-hour VGOS R&D sessions and six 1-hour tests were placed in the Master Schedule. These are summarized in Table 1.

Table 1 VGOS R&D sessions.

Observing date	Session code	Duration (hours)	Integrations (seconds)	Frequency sequence
2021-07-29	VR2101	24	7–20	Standard
2021-10-15	V1288A	0.5	60	New
2021-10-15	V1288B	0.5	60	New
2022-01-20	VR2201	24	7–20	Standard
2022-02-18	VT2049	1	7–20	V1288A
2022-03-17	VR2202	24	7–20	V1288A
2022-03-18	VT2077	1	5–18	Standard
2022-05-19	VR2203	24	7–20	Standard
2022-07-21	VR2204	24	5–18	Standard
2022-07-22	VT2203	1	120	New
2022-09-15	VR2205	24	7–20	Standard
2022-09-16	VT2259	1	120	New
2022-11-09	VR2206	24	7–20	New
2022-11-10	VT2314	1	?	?

3 Frequency Sequence Development

The current operational VGOS frequency sequence was developed in support of the GGAO–Westford proof of concept sessions. Now, after several years, the VGOS network has expanded and RFI problems have become more ubiquitous. A review of the frequency sequence has been undertaken.

Two basic tendencies are required of a good frequency sequence: 1) that the SNR for fringe detection is as low as possible; and 2) that delay precision is as high as possible. In general, delay precision improves as channel separation increases and fringe detection improves as channel distribution becomes more even.

These tendencies are tempered by hardware constraints. To ensure network compatibility, a system with four 512-MHz bands across 3 to 10.7 GHz (the same as for the proof-of-concept system) will be considered the benchmark.

In addition, other factors must be considered, e.g., the loss of channels due to narrow-band RFI, the loss of whole regions of the spectrum due to broadband RFI, non-linear behavior of the system, and non-linear behavior caused by source structure.

In the design process used here, it is assumed that band-A and band-D will be placed as near as possible to the extremes of the 3 to 10.7 GHz frequency range. This is to ensure adequate delay precision. To study the detectability aspect of the sequences, the probability of a missed phase connection is then calculated at every possible pair of band-B and band-C frequencies as they are moved, in 32-MHz steps, throughout the intervening spectral region.

In Figure 1, log_{10} of the best (i.e., lowest) 8,000 probabilities are plotted assuming an SNR of 10 in each band. At this SNR, it can be seen that there is a wide range of sequences that perform well, e.g., for sequences in the blue and green regions the probability of error is less than 1 part in 10^5. The existence of these somewhat broad regions means that, at least to some extent, frequencies can be adjusted to avoid broadband RFI.

The best performing sequence (located at f=[3,000.4; 4,472.4; 6,584.4; 10,200.4] MHz) has been tested in two 1-hour sessions, V1288A, VT2049, and in one 24-hour session, VR2202. In the sessions correlated so far, no serious RFI issues were detected although not all stations were included in the tests. Detailed RFI analysis at each station will be required for a more definitive and robust sequence definition.

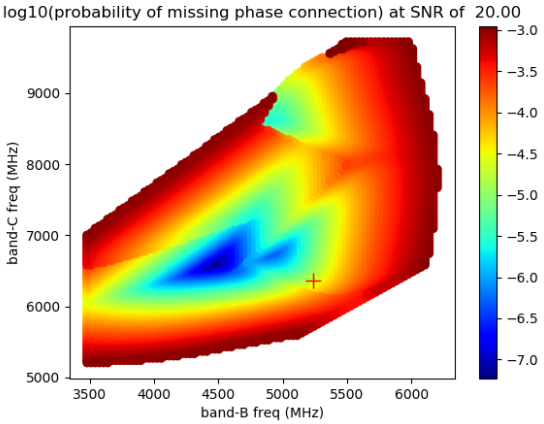

Fig. 1 Log_{10} of the probability of a phase connection error at SNR=20. The + symbol represents the position of the current VGOS sequence.

Intuitively, it is expected that sequences will perform reasonably well even if a small number of channels are lost. With the current VGOS mode using 8-Gbps recording, 50% of each band is occupied, which provides significant redundancy. This was verified numerically for pairs of channels (Figure 2). The red trace represents the Delay Resolution Function (DRF) for the V1288A sequence, while each green trace represents the DRF for the same sequence but with the loss of two channels. All possible combinations of channel pairs were considered. In addition to the loss of about 3% SNR (which is not reflected in the figure), the DRFs are distorted somewhat but not enough to significantly degrade fringe detection.

Finally, the impact of nonlinear phase is considered in a numerical study. The phase of a single VGOS band is offset and this is repeated in sequence for each of the four bands. In all cases, the phase offset produces a noticeable shift of the main peak of the DRF (which manifests as an unwanted delay bias). However, for band-B or band-C, the delay bias is also accompanied by a significant distortion of the DRF which greatly increases the probability of a sub-ambiguity error. For the sequence used in V1288A and a phase offset of 45°, the height of the highest sidelobe is nearly as high as the main peak (Figure 3). This emphasizes the importance of careful calibration of the system phase and the danger of using sources with excessive structure.

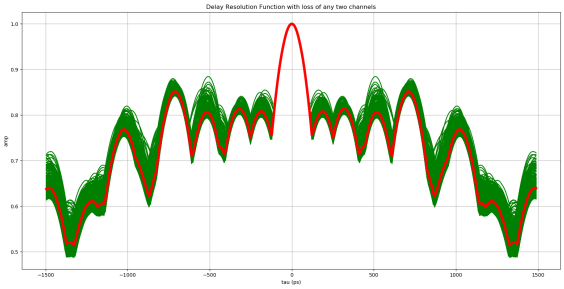

Fig. 2 DRFs of the V1288A sequence. Green traces assume the loss of arbitrary pairs of channels. Horizontal grid lines are separated by 10% of the central peak and vertical grid lines are separated by 500 ps.

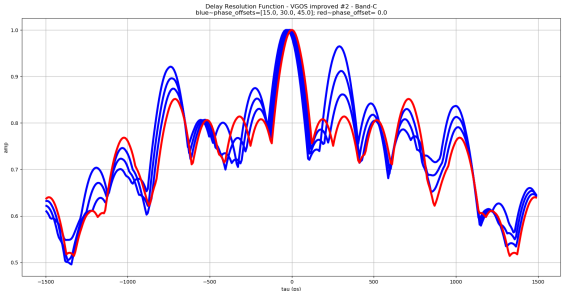

Fig. 3 DRFs of the V1288a sequence. Blue traces represent DRFs for phase offsets of 15°, 30°, and 45° at band-C. The red trace is for no phase offset. Horizontal grid lines are separated by 10% of the central peak and vertical grid lines are separated by 500 ps.

4 Scheduling

The VGOS R&D sessions are scheduled using VieSched++ [3] with the session designed individually.

The main focus of the R&D sessions is to increase the observing rate, i.e., the number of observations per session at each station. This is accomplished primarily through the following scheduling-related strategies:

- Two (instead of one) record modules are used at the Mark-6 stations. This ensures that data can be recorded in real-time without waiting for a record buffer to flush. The resulting saving is significant given that, with the current VGOS single module mode, the "buffer flush" is equal in duration to the data record time.
- The accuracy of the antenna slew models was confirmed; if necessary they were improved. This ensures that the scheduling software accurately predicts on-source arrival time so that antennas are neither needlessly waiting for observations to begin nor arriving too late. The Onsala case was particularly interesting where it was discovered that slew rate can change depending on antenna pointing angle and slew direction.
- Field system procedures (preob and midob) were streamlined, removing unnecessary and time-consuming checks. As a result, the preob time was reduced from four seconds to two seconds.
- Signal-to-Noise (SNR)-based scheduling, similar to that developed for some early EU-VGOS sessions [1], was used. With this approach, the integration time is adjusted, within limits, to achieve a specified SNR. For the R&D sessions, the integration time limits were either from 7 seconds to 20 seconds or from 5 seconds to 18 seconds (see Table 1 for details). This is in contrast to operational VGOS sessions where fixed 30-s integrations are used. SNR calculations require accurate system SEFDs and source fluxes. Since source fluxes are not available at the VGOS band frequencies, S/X flux densities were inter-/extrapolated to VGOS frequencies assuming a power-law spectral index. For VR2203, the first VGOS-based band-ABCD source flux density catalog, derived from previous VGOS sessions, was tested. Also, the R&D SNRs were typically too low for good calibration. As a result, calibration scans were inserted into the schedules. The cadence was either every hour or every two hours and the duration was either 60 seconds or 120 seconds (see Table 2 for details).

Table 2 VGOS R&D scheduling statistics. Columns: session name, number of stations, number of observations, number of scans, and number of sources.

Session code	#sta	#obs	#scans	#src	Cal. scans # | duration	Source catalog
VR2101	7	25,619	3,397	94	24 | 120 s	S/X-based
VR2201	9	36,644	4,352	176	12 | 60 s	S/X-based
VR2202	9	37,701	3,707	141	12 | 60 s	S/X-based
VR2203	8	26,840	4,295	90	24 | 60 s	VGOS ABCD

Each R&D session has its own targets and strategies, e.g.:

- VR2101 is the first VGOS R&D session to use SNR-based scheduling. Additionally, the schedul-

ing algorithm tried to include only sources that are observed in at least ten scans. This was done utilizing iterative source selection as discussed in [3].

- VR2201 set the minimum and target number of scans per source to ten and 22, respectively, to put even more emphasis on a better distribution of scans among sources. Based on the target number of scans and the network source visibility, a minimum time between two scans to the same source was calculated. This was done for each source. [Note that fillin-modes and other scheduling algorithms could still cause some sources to be observed more frequently.] As a result, the number of scheduled sources was increased to 176, with an average number of scans per source of 24.8 ± 7.8. Additionally, for the first time, a southern-hemisphere station, HOBART12, was included in tagalong mode. To ensure good inclusion, the tagalong mode was improved by a second round of fillin-mode scans, the so-called fillin-mode a posteriori. As a result, HOBART12 was scheduled in over 1,000 scans despite its remote location and tagalong status. Finally, VR2201 included one pair of radio sources scheduled 27 times in phase-referencing mode.
- VR2202 put slightly less emphasis on the distribution of scans among sources in favor of improving good short-term station sky coverage. This was done to enable a better estimation of high-frequency tropospheric disturbances. To achieve this, the Monte-Carlo simulation approach was adjusted to include high-frequency troposphere estimates. Additionally, the station-dependent sky coverage optimization parameters were utilized to account for the different antenna slew rates and sky visibilities.
- VR2203 used, for the first time, a VGOS frequency source flux density catalog for the calculation of the SNR-based integration times. In addition, the minimum time between two scans to the same source was lowered to 20 minutes to obtain more scans per source.

5 Source Structure and Modeling

For VGOS, the first image processing task is to fit Gaussian components based on closure phases and closure amplitudes. This can be divided into three steps. First, isotropic total variation regularization is applied, which favors the smoothness of the flux density distribution to solve the ill-posed problem in imaging, to obtain a map of flux densities on any predefined pixels [4]. The process can be called closure imaging [5]. Secondly, we use these "closure" maps to self-calibrate visibilities. Finally, the Gaussian components are fitted from these self-calibrated visibilities.

The second task is to determine the total flux densities of the maps if there is amplitude calibration information available for a fraction of the antennas but not necessarily for all the antennas. This is necessary because the amplitudes were not calibrated based on the SEFD and antenna gain curves, leading to the closure maps missing a correct scale of the total flux densities. Even though this scale itself does not affect the derived corrections for source structure, it is important to determine the correct total flux density for an image so that we can predict SNR in scheduling.

Aligning the images over frequency is the third task. The information of the phase center is lost in imaging due to difficulties in calibrating the visibility phases; note that this is a common problem in VLBI imaging rather than a unique issue for the closure imaging. To derive coherent visibility phases, like that of a point source, by correcting structure phases based on the four-band maps, the phase centers of these four maps must be accurately linked with each other [6].

The imaging results for VGOS R&D session VR2101 are publicly available[1], where we report the statistics of closure imaging, maps, and models of Gaussian components, and the preliminary results of the model corrections. Table 3 summarizes the imaging results. Out of the 28 imaged sources, only eight sources do not have a second bright component ($> 30\%$ to the peak) at any of the four bands.

For VGOS R&D session VR2201, we have imaged 106 sources. The Gaussian components can be determined for 103 sources, a demonstration of a significant improvement in the imaging capability. This session allows for many of the low-declination sources to be imaged, as shown in Figure 4 for source 0748+126.

The on-going work includes the second and the third tasks of the imaging process, and challenges can be foreseen in particular for the image alignment. A common issue is that parts of the jet components may

[1] `http://www.metsahovi.fi/~xum2/me/vr2101/`

Table 3 Number of the Gaussian components and the flux density ratio of the second bright component to the peak component based on the observations from VGOS R&D session VR2101.

Source	3.3 GHz		5.5 GHz		6.6 GHz		10.5 GHz	
	$N_{\rm cmp}$	$R_{\rm flux}$	$N_{\rm cmp}$	$R_{\rm flux}$	$N_{\rm cmp}$	$R_{\rm flux}$	$N_{\rm cmp}$	$R_{\rm flux}$
0016+731	2	0.93	3	0.38	3	0.38	3	0.34
0059+581	2	0.08	2	0.80	2	0.98	2	0.73
0133+476	2	0.14	2	0.19	2	0.17	2	0.11
0202+319	2	0.32	2	0.16	2	0.15	2	0.86
0235+164	1	—	1	—	1	—	2	0.01
0529+483	2	0.08	3	0.81	3	0.94	3	0.03
0552+398	1	—	2	0.65	2	0.81	2	0.87
0613+570	1	—	2	0.58	2	0.10	2	0.14
0716+714	2	0.12	2	0.13	2	0.17	2	0.15
0748+126	3	0.45	3	0.41	3	0.22	2	0.13
0805+410	2	0.05	2	0.07	2	0.13	2	0.09
0955+476	2	0.20	2	0.12	2	0.11	2	0.03
1144+402	2	0.59	2	0.62	2	0.54	2	0.13
1156+295	2	0.11	2	0.08	2	0.08	2	0.04
1606+106	3	0.82	3	0.45	3	0.50	3	0.35
1749+096	2	0.23	2	0.58	2	0.06	2	0.21
1751+288	2	0.07	2	0.05	1	—	1	—
1803+784	3	0.45	2	0.28	4	0.35	3	0.30
1849+670	3	0.11	2	0.12	2	0.09	2	0.35
2000+472	2	0.62	2	0.12	2	0.66	3	0.81
2059+034	2	0.08	2	0.18	2	0.18	2	0.06
2113+293	2	0.09	2	0.29	2	0.11	2	0.39
2215+150	1	—	1	—	1	—	2	0.46
2229+695	2	0.52	3	0.28	3	0.20	3	0.28
NRAO150	3	0.50	1	—	1	—	2	0.64
OJ287	3	0.82	3	0.63	5	0.96	3	0.68
3C371	2	0.40	3	0.86	3	0.65	3	0.40
3C418	3	0.42	3	0.53	2	0.50	3	0.44

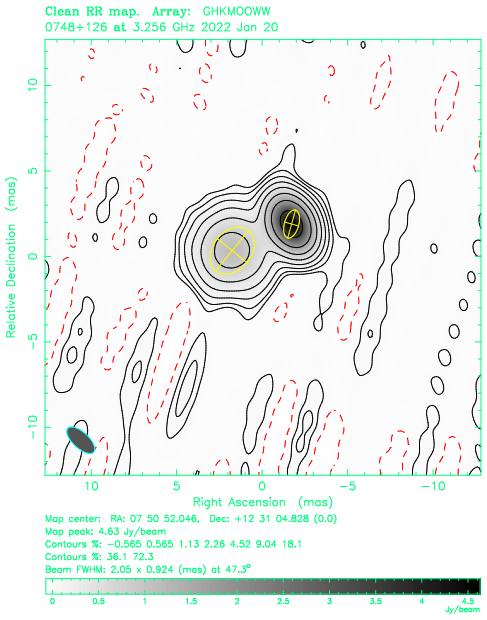

Fig. 4 VGOS image of source 0748+126 at 3.3 GHz from R&D session VR2201 (January 20, 2022). The Gaussian components are shown as the yellow ellipses.

contribute to the modeled core and change its position. Due to the large difference in the angular resolutions across the four bands, the "core" position will move towards the jet by a different offset at each of the four bands. The differences in the u,v coverage of a given source from session to session can also affect the stability of the image alignment over time.

References

1. F. Jaron, S. Bernhart, J. Böhm, J. González Gracía, J. Gruber, Y.K. Choi, I. Martí-Vidal, M. Schartner, B. Soja, J. Wagner, E. Varenius, H. Verkouter, on behalf of the EU-VGOS collaboration, "EU-VGOS activities in Vienna," Proceedings of the 25th European VLBI Group for Geodesy and Astrometry Working Meeting, 2021, ISBN: 978-91-88041-41-8
2. B. Petrachenko, A. Niell, D. Behrend, B. Corey, J. Böhm, P. Charlot, A. Collioud, J. Gipson, R. Haas, T. Hobiger, Y. Koyama, D. MacMillan, Z. Malkin, T. Nilsson, A. Pany, G. Tuccari, A. Whitney, J. Wresnik, "Design aspects of the VLBI2010 system," Progress report of the IVS VLBI2010 Committee, NASA/TM-2009-214180, 2009. https://ivscc.gsfc.nasa.gov/publications/misc/TM-2009-214180.pdf
3. M. Schartner and J. Böhm, "VieSched++: A New VLBI Scheduling Software for Geodesy and Astrometry," Publications of the Astronomical Society of the Pacific, vol. 131, no. 1002. IOP Publishing, p. 084501, Jun. 18, 2019. doi: 10.1088/1538-3873/ab1820.
4. Xu M. H., Savolainen T., Zubko N., Poutanen M., Lunz S., Schuh H., Wang G. L., "Imaging VGOS Observations and Investigating Source Structure Effects," 2021, Journal of Geophysical Research (Solid Earth), 126, e21238. doi:10.1029/2020JB021238
5. Chael, A. A., Johnson, M. D., Bouman, K. L., Blackburn, L. L., Akiyama, K., and Narayan, R., "Interferometric Imaging Directly with Closure Phases and Closure Amplitudes," The Astrophysical Journal, vol. 857, no. 1, 2018. doi:10.3847/1538-4357/aab6a8
6. Xu M. H., Savolainen T., Anderson J. M., Kareinen N., Zubko N., Lunz S., Schuh H., "Impacts of the image alignment over frequency for VLBI Global Observing System," A&A, 663 A83 (2022), doi: https://doi.org/10.1051/0004-6361/202140840